Chapter 4

Spin Distribution Measurements

From the analysis of the measured excitation functions (EFs) and forward recoil range distributions (FRRDs) data of the populated radio-nuclides, in heavy- ion induced reactions at projectile energy between 3-8 MeV/nucleon, it has been observed that incomplete fusion plays an important role and the break-up of the projectile in α- clusters takes place, as it approaches the target nuclear field. A significant enhancement in the measured EFs over fusion-evaporation (CF) model code PACE-2 predictions have been obtained in α-particle emission channels. These enhancements have been attributed to incomplete fusion (ICF) of the projectile with the target. It has been observed from the FRRDs of the residues populated in break-up α-emission channels that a partial linear momentum transfer (LMT) takes place due to fusion of the projectile-fragment with the target and hence their peaks have been observed at relatively shorter distance in the recoiling medium, than the residues produced in complete fusion channels. Studies show that incomplete fusion (ICF) process plays an important role in understanding the reaction dynamics. However, the information regarding multiplicity of driving input angular momentum associated with CF and ICF could not be drawn simply from the measurement of EFs and FRRDs. For the better understanding of underlying processes, changed particle-γ coincidence technique has been applied to perform an experiment, where qualitative information about driving input angular momentum associated via CF and ICF have been obtained at 5.6 MeV/nucleon energy for $^{16}O + ^{160}Gd$ system. Spin distribution studies i.e., the study of qualitative behaviour of intensity profiles with observed spin of the residues populated in CF and ICF have been done to extract the

information about input angular momentum and the $\ell-$window assigned for these processes. Spin distributions of CF and ICF are expected to be distinctly different. Moreover, side-feeding of γ-ray intensities have been deduced from the experimentally measured spin-distribututions. Experimental details and out come of the result, has been discussed here.

4.1 Experimental Details

In order to obtain the multiplicity of driving input angular momentum associated with CF and ICF reaction dynamics, charged particle-γ coincidence technique has been applied to perform an experiment with ^{16}O + ^{160}Gd system at beam energy ~ 5.6 MeV/ nucleon, at Inter-University Accelerator Centre (IUAC), New Delhi, India. In this experiment, 'Gamma Detector Array' (GDA) along with 'Charged Particle Detector Array' (CPDA) has been used. Coincidences were recorded between prompt gamma-rays and charged particles (Z=1,2). A brief description of target preparation, experimental set-up, electronics used, target irradiation, data analysis, results and its interpretations are given in following sub-sections;

4.1.1 Target preparation

The enriched target ^{160}Gd (enrichment ~ 98.2%) available in the form of metallic rod has been used to prepare target of thickness ~ 1.3 mg/cm^2 by rolling machine at Target Laboratory of IUAC, New Delhi, India. The thickness of the target has been measured by α-transmission method by using the ^{241}Am source. In order to check the uniformity of the sample, thickness of the sample was measured at the different places. The target was cut into the size of 1.2 × 1.2 cm^2 pasted on the rectangular Al-target holder having central hole of 10 mm diameter. The aluminum target holders were used for rapid heat dissipation.

4.1.2 The experimental set-up

Gamma Detector Array (GDA) in conjunction with Charged Particle Detector Array (CPDA) has been used for the present charged particle-γ coincidence experiment at IUAC, New Delhi, India. The Gamma Detector Array (GDA) consisting of 12 HPGe detectors to detect γ- rays and the Charged Particle Detector Array (CPDA) consisting of 14 Phoswich plastic detectors, used to detect proton and alpha particles. A brief description of GDA and CPDA set-up has been given in following sub-sections.

Gamma Detector Array (GDA)

The Gamma Detector Array (GDA) is high counting efficiency dedicated system installed at Inter-University Accelerator Centre (IUAC), New Delhi used for nuclear structure and nuclear reaction studies. The array consists of 12 Compton suppressed n-type HPGe detectors. In this array, the HPGe detectors along with the Anti-Compton Shields (ACS) are mounted on two rigid mechanical structures on either side of the 30^0 beam line. These structures are movable with the help of rails fixed on the floor. Each structure consists with six detectors in the two rows, 25^0 above and below the horizontal plane with three detectors in each row at 45^0, 99^0 and 153^0 in-plane angles. The Anti-Compton Shields (ACS) is cone-shaped, with a 146 mm deep hole of 72 mm diameter for inserting the detectors and a tapered axial opening for entry of the photons. Side view of the GDA set-up at IUAC, New Delhi has been shown in Fig.4.1.

The target was housed in the centre of Charged Particle Detector Array (CPDA) chamber and was surrounded by GDA in GDA+CPDA configuration. The chamber is made up of aluminum as to minimize the absorption of emitted γ-rays from the target area. The CPDA chamber has two rotatable flanges for the beam-line alignment purpose. Special care has been taken to get the centers of the CPDA and GDA coincide. The CPDA is held and aligned by the top and bottom flanges of the target chamber. Specially

designed set of two flanges hold each set of 7 charged particle detectors in a proper geometry to reproduce the center.

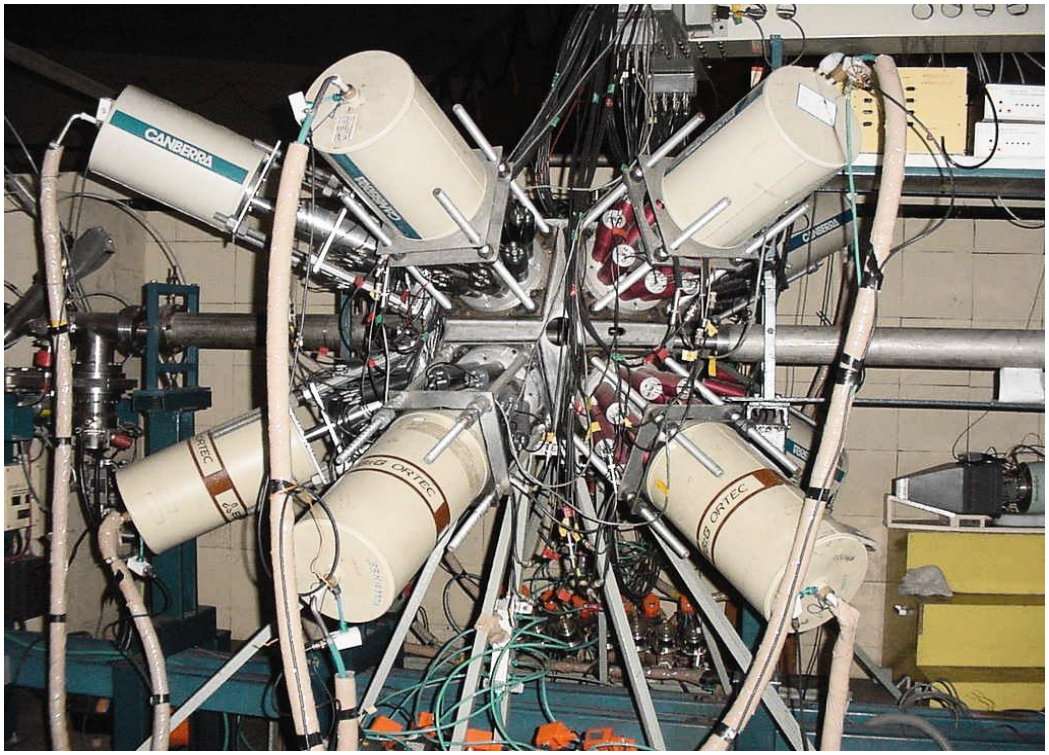

Fig. 4.1: The side view of Gamma Detector Array (GDA) at IUAC.

Charged Particle Detector Array (CPDA)

The charged particle detector array (CPDA) in conjunction with the 12 HPGe detectors of Gamma Detector Array (GDA) has been used in the present experiment. The Charged Particle Detector Array (CPDA) at Inter-University Accelerator Centre, New Delhi consists of the 14 charged particle detectors (Phoswich plastic scintillators) arranged in two truncated hexagonal pyramids. The bases of the all pyramids are in the horizontal plane with each other having trapezoidal shape. The two hexagonal detectors are inserted from the top and bottom. The total solid angle coverage is greater than 90%

of 4π taking into account the opening for beam entrance and exit. The full CPDA is held in place from the top and bottom flanges of the scattering chamber as shown in Fig.4.2. The corners of the trapezoids are cut-off for the entrance and exit of the beam and for target support purpose. The light collection is done by properly shaped UVT light guides coupled to 25 mm diameter miniature phototubes. There are six detectors around 90^0, four detectors in the forward angles (10^0- 60^0) and four in backward angles (120^0-170^0). The specific features of CPDA are summarized in Table 4.1.

4.1.3 On-line target irradiation

In the present on-line experiment, a continuous irradiation has been carried out in a special designed aluminum made vacuum chamber of 16 cm diameter, where seven charge particle detectors (CPDs) from top-side and seven CPDs from bottom-side are housed. The scattering chamber consisting of the fourteen CPDs, surrounded by

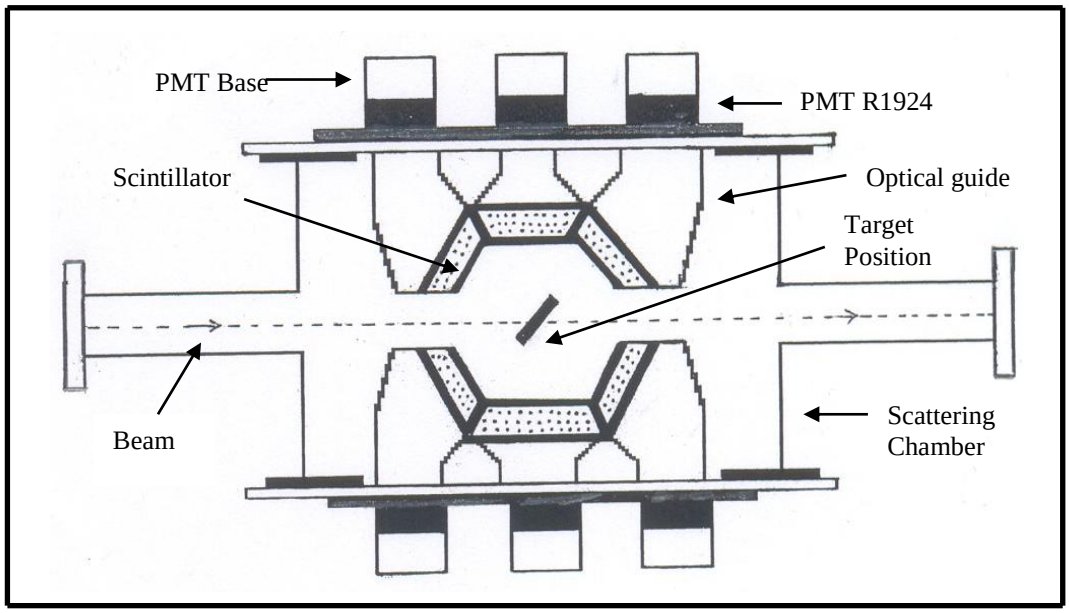

Fig. 4.2: A schematic layout of the scattering chamber housing Charged Particle Detector Array (CPDA).

Table 4.1: Salient features of Charged Particle Detector Array (CPDA).

Geometry of CPDA	Two truncated hexagonal pyramid
Detector Material	Phoswich Plastic scintillator
Solid angle covered	90% of 4π
Number of detectors	14
Target to detector distance	6 cm
Typical count rate for individual	50,000 counts per second
ΔE detector	BC400, thickness ~ 100 μm
E detector	BC444, thickness ~ 5 mm
Optical guide	BC800, UVT Lucite material
PMT	1'' diameter, R1924 - HAMAMATSU
Glue for PMT & optical guide	Optical cement (BC 600)

twelve Compton suppressed HPGe detectors. Special care has been taken so that centre of the CPDA and that of GDA coincide. This chamber has two rotatable flanges for the alignment purposes. The self-supporting ^{160}Gd target of thickness about 1.3 mg/cm^2 was mounted over the target ladder, placed at 45^0 with respect to the beam direction in the scattering chamber. The ^{160}Gd target was bombarded by $^{16}O^{+7}$ beam at energy ~5.6 MeV/nucleon with beam current ~ 25 nA delivered from 15UD-Pelletron Accelerator at IUAC. Coincidences between charged particle (Z=1, 2) and prompt γ-rays have been recorded using GDA along with CPDA set-up. As described earlier, GDA is an assembly of 12 Compton suppressed HPGe detector at 45^0, 99^0 and 153^0 with respect to the beam direction in an arrangement of four detectors at each angle. For the coincidence purpose, all fourteen CPDA have been divided into three angular zones. There are four detectors in the forward angles (F) ($10\text{-}60^0$), four in backward angles (B) at ($120\text{-}170^0$) and six detectors side ways (S) i.e., around 90^0 i.e., at ($60^0\text{-}120^0$), covering nearly 90% of the

total solid angle so that the angular distribution of particles in $\approx 4\pi$ arrangement may be recorded. In the forward direction, detectors were supposed to detect both (i) fusion-evaporation (CF) α-particles (of energy ~17 MeV), emitted from the decay of compound nucleus $^{176}Hf^{*}$ after statistical equilibrium is achieved, and (ii) 'direct' or 'fast' α-particles (of energy ~ 25 MeV), moving as spectator, associated with ICF of the projectile. As such, in order to record 'direct' or 'fast' α-particle originated from ICF reaction in forward cone, an Al-absorber of appropriate thickness (~ 100 μm) has been placed in front of the each four charged particle detectors (CPDs), to stop the fusion-evaporation α-particles, produced in 'complete fusion' so that only 'direct' or 'incompletely fused' α-particles may be detected. ^{16}O-ion beam was finally stopped on a thick tantalum sheet attached with Faraday cup in the end of beam line. All the HPGe detectors were calibrated by the using ^{133}Ba, ^{60}Co and ^{152}Eu-source of known strength. The efficiency of the high resolution HPGe detector was measured by using ^{152}Eu-source at the target position. Moreover, ^{241}Am source has been used to calibrate the detectors in CPDA. The particle(s) (protons or αparticles) observed from the break-up of the projectile can be detected in coincidence with the prompt gamma- rays in the forward direction leading to the ICF reaction. A typical sectional view of detectors arrangement in CPDA + GDA configuration is shown in Fig.4.3.

4.1.4 Experimental procedure and Electronics

In the present in-beam particle-gamma coincidence experiment we have measured relative yields of the evaporated residues (ERs) in coincidence with charged particles (α, p) in forward and backward directions for the system ^{16}O + ^{160}Gd at 90 MeV. The target was bombarded with the average beam current of about ~ 25 nA**.** Two current integrators were used to read the current on collimator and Faraday cup for beam focusing purpose on the target. The current was minimized on the collimator and maximized on the Faraday cup for the proper focusing and alignment of the beam. The

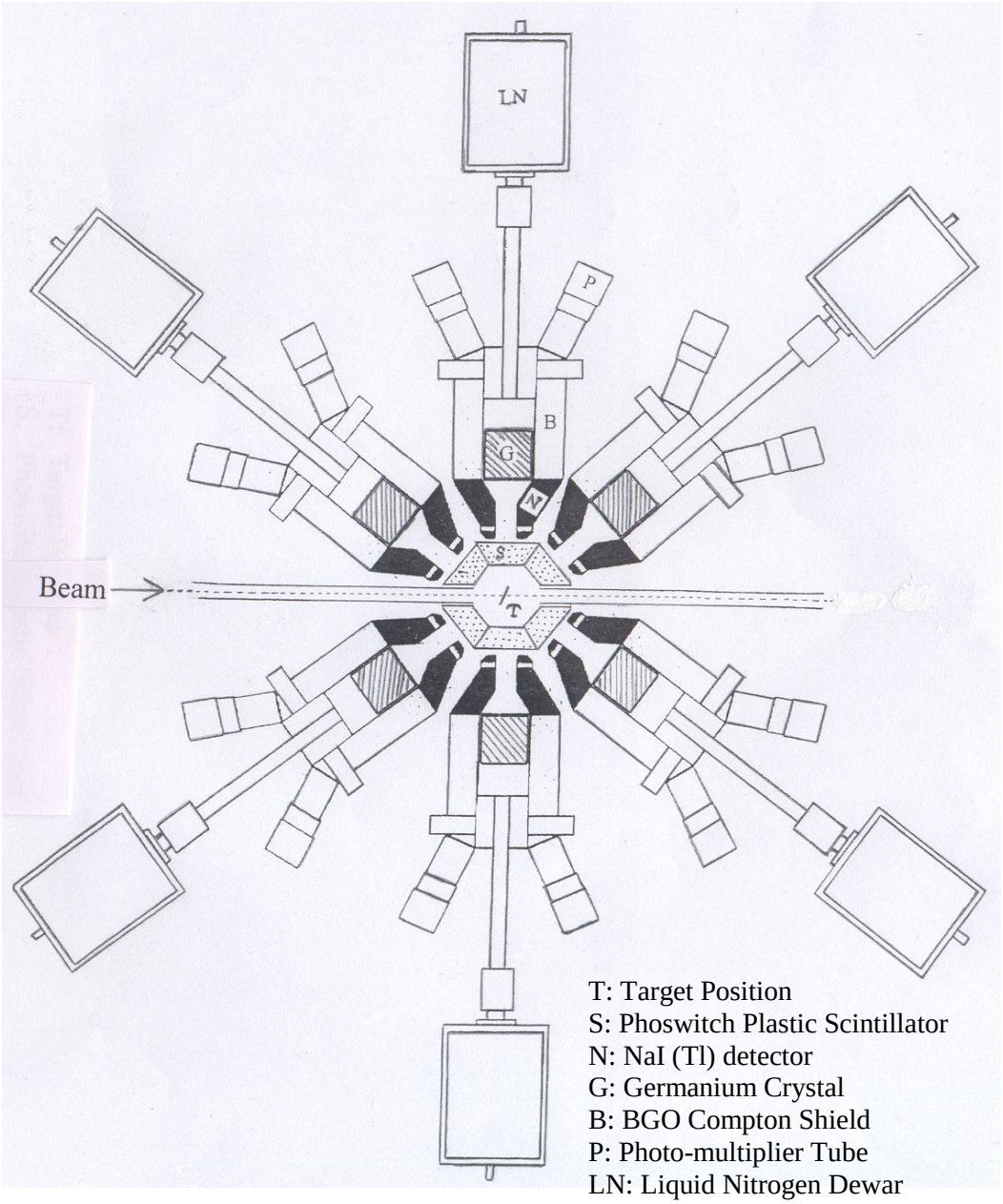

Fig. 4.3: A typical sectional view of detectors arrangement in CPDA + GDA configuration.

CAMAC crates were used for the interfacing. The on-line multi-parameter data were recorded by the data acquisition software CANDLE [1] in event-by-event LIST mode and stored them in computer hard disk. Each event is registered with the following parameters:

(i) The timing of all the detectors from TDC module,

(ii) The charged particle and α-particle multiplicity,

(iii) Twelve energy signals from each of the twelve HPGe detectors, satisfying all the coincidence and anti-coincidence relations.

The timing information from HPGe detectors is recorded by using a 16 channel CAMAC Time-to-Digital Converter (TDC). Timing spectra are recorded under six gating conditions, P-forward, α-forward, P-90^0, α-90^0, P-backward and α-backward in CPDA. Particles (alphas and protons) identification has been done based on pulse height of the signal from fast-slow plastic Phoswich charged particle detectors. The block diagrams of CPDA electronics are shown in Fig. 4.4 and Fig. 4.5. These circuits were used to record multiplicity of all charged particles and α-particles, detected in the CPDA. The signals from each of the charged particle detector are fed into 16 channel fast amplifier (PHILIPS 776), which amplifies the CPD signals with amplification factor ($\times$10). The output of the fast amplifiers are fed to the variable gain amplifiers (PHILIPS 777), which are used for further amplification to match the gain of all the detector signals. Multi-unit constant fraction discriminators (ORTEC CFD 8000) are used to adjust the threshold of CPDA channels for the differentiation of the particles (p,α) and are set by the variable gain amplifier output on an oscilloscope triggered by the CFD output. For the particle (p,α) condition the threshold of the CFD was set just above the noise (~ 20 keV). The threshold of the alpha particles was fixed just above the proton signal height. These modules give a multiplicity (M) signal and OR signal. The output signals multiplicity (M) and OR is fed to the linear gate Fan-in / Fan-out (PHILIPS 744

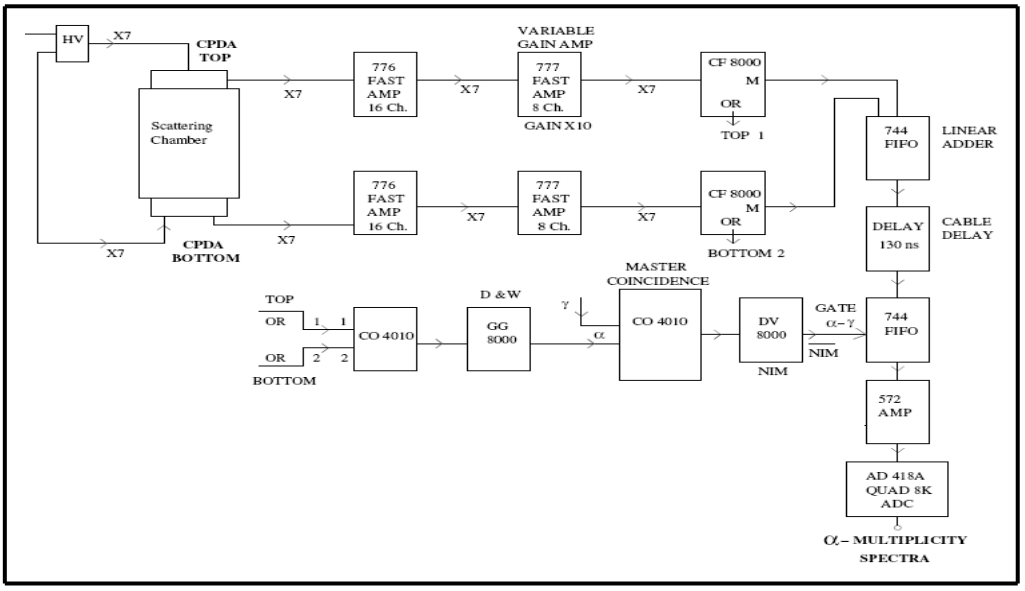

Fig. 4.4: The block diagram of the electronics used for α-particle multiplicity spectra.

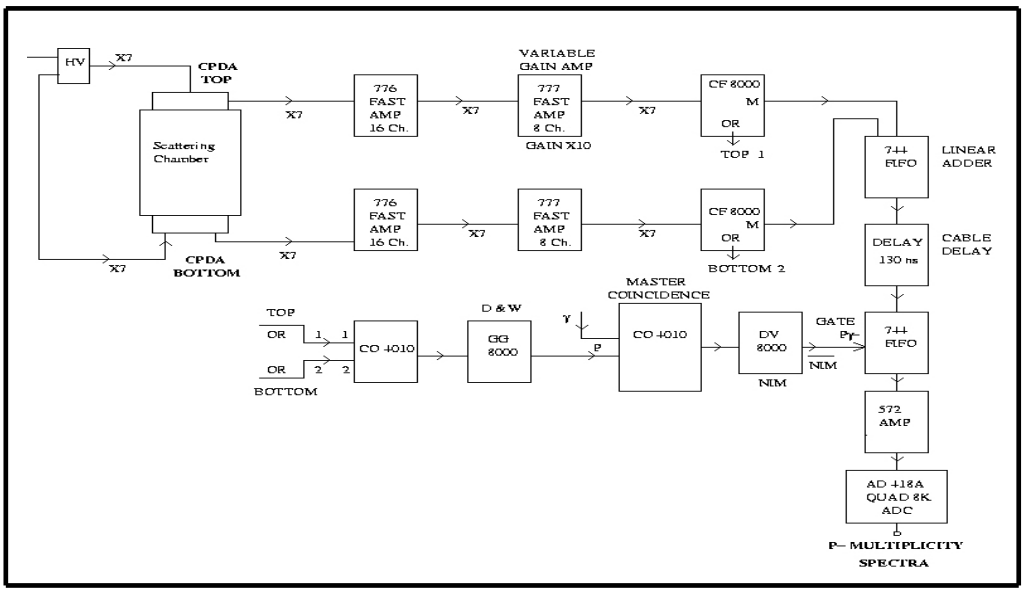

Fig. 4.5: The block diagram of the electronics used for charged particle multiplicity spectra.

FIFO) and a coincidence unit (4 fold 4 input logic CO 4010). The coincidence logic unit is to generate a logic output and module FIFO gives many outputs. The output of FIFO is delayed by ≈130 ns and then goes to 744 FIFO module. The logic output from the coincidence unit goes to delay generator (GG 8000) to adjust the depth and width of the signal. This is fed into the same coincidence module and demanding master coincidence in between α-particle and γ-rays. The output from the coincidence module is fed into a variable delay generator (DV 8000). The NIM signal is fed to the trigger logic unit to generate the α-γ gate. After proper delay and width adjustment by depth and width generator, output goes to linear gate Fan-in / Fan-out (PHILIPS 744 FIFO). The output of the 744 FIFO goes to the amplifier (ORTEC 572). The amplified signal from the amplifier is fed into the analog-to-digital converter (8 K, 14 bit ADC) for recording the α-multiplicity and P-multiplicity spectra. It is used mainly to record the multiplicity of charged particles and α-particles detected in the CPDA. The multiplicity of charged particles and α-particles are taken to define the charged particle-γ-coincidence. The γ-rays in coincidence with the charged particles as well as α-particles are measured using high-resolution HPGe detectors at angles 45^0, 99^0, 153^0. Particle-like-fragments (PLFs) are registered at three angular ranges, forward angles (10^0-60^0), backward angles (120^0-170^0) and sideways at 90^0 by detectors in CPDA. Over all, six gated γ-ray spectra in coincidence with charged particles (P) and α-particles in three different angular zones were recorded:

(i) Particles (P) in forward (F) direction i.e., in (10^0-60^0) angular zone
(ii) Particles (P) in side ways (S) direction i.e., in (60^0-120^0) angular zone
(iii) Particles (P) in backward (B) direction i.e., in (120^0-170^0) angular zone
(iv) α-particles (α) in forward (F) direction i.e., in (10^0-60^0) angular zone
(v) α-particles (α) in sideways (S) direction i.e., in (60^0-120^0) angular zone
(vi) α-particles (α) in backward (B) direction i.e., in (120^0-170^0) angular zone

Apart from the coincidence spectra, under different gating conditions, defined above, the data have also been collected in 'Singles mode' without any condition. The neutron channels have been identified by looking into 'singles spectra' during the analysis.

4.2 Off-line Data Analysis and Results

After recoding the data in event-by-event LIST mode in the computer hard disc with UNIX operating system, the off-line data analysis has been done. Sorting of the data, subsequent projection of spectrum and the γ-ray photo-peak fittings were done by using the software INGASORT [2]. The sorting of list mode data has been processed through a series of steps before the final spectrum could be generated. The gains of the all ADCs were approximately matched during the experiment, but a precise gain matching was needed in order to add the projected spectra of all the HPGe detectors. The gain matching has been done using the γ-sources ^{152}Eu and ^{133}Ba, to cover the energy range of 80-1408 keV. The gated spectrum for gamma rays detected in a particular detector was obtained by summing up all the events in all the other detectors, which are in coincidence with that charged particle. Each γ-ray rides over a background and the contribution to the gated spectra has been subtracted from the final gated spectra. In order to improve the data statistics, assuming the angular distribution of the observed γ-rays to be isotropic, all the gated spectra for a particular gating condition have been summed up. Projecting different gating conditions, discussed earlier, like P-forward, α-forward, P-90^0, α-90^0, P-backward and α-backward of CPDA detectors, the analysis of the gated gamma-spectra has been done. The observed γ-ray singles spectrum has been shown in Fig. 4.6, and γ-ray gated spectra in coincidence with alphas in forward cone (AF), alphas in backward cone (AB) , Particles in forward cone (PF) and Particle in backward cone (PB) have been recorded and shown in Figs. 4.7-4.10 respectively. Singles spectrum has been recorded to identify the neutrons emission channels, which are identified as the CF products.

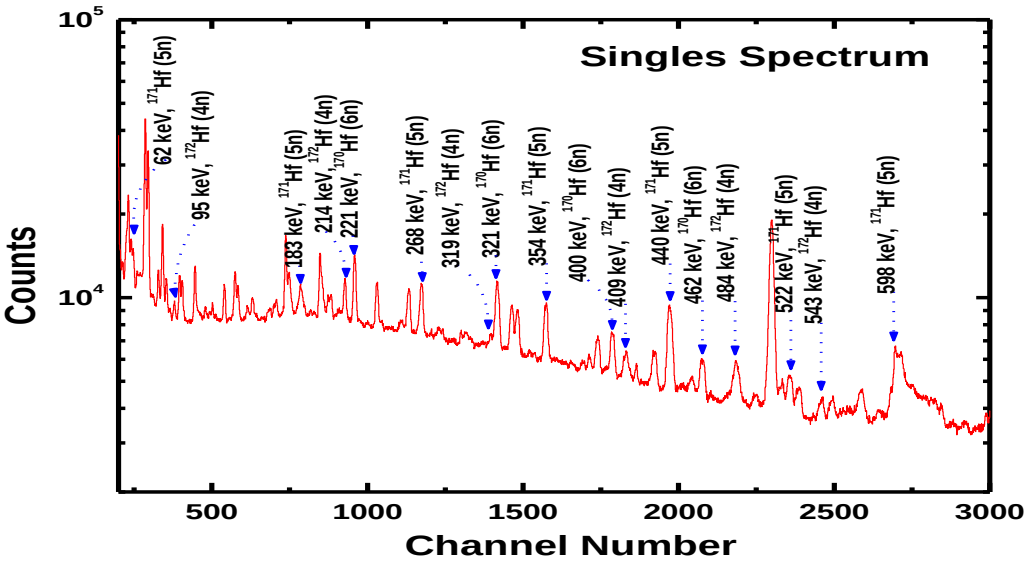

Fig. 4.6: A typical γ-ray spectrum in singles mode (without gating condition) for ^{16}O + ^{160}Gd system at energy, E ~ 5.6 MeV/nucleon. Peaks have been assigned to different neutrons channels, which are populated via CF process.

The data analysis has been done in two steps by using software INGASORT [2]. In the first step, xn-channels (as mentioned above) have been identified from singles data taken from the best Ge-detectors. As a matter of confidence, these neutrons channels have been confirmed by the identification of their characteristic γ-rays from the decay singles spectra recorded time-to-time during the experiment without beam. However, in the second step, four coincidence gating conditions like α-Forward, α-Backward P-Forward and P-Backward on all the observed γ-ray energy spectra have been applied and identification of CF and ICF reaction products has been done. α/ 2α-emission channels populated via CF reaction have been identified from the backward alpha and particle-gated spectra. As per kinematical definition of ICF, fast α-particle is produced in ICF reaction and is expected to flow only in the forward cone. As such, ICF reaction products populated via αxn/2αxn-emission channels have been identified from

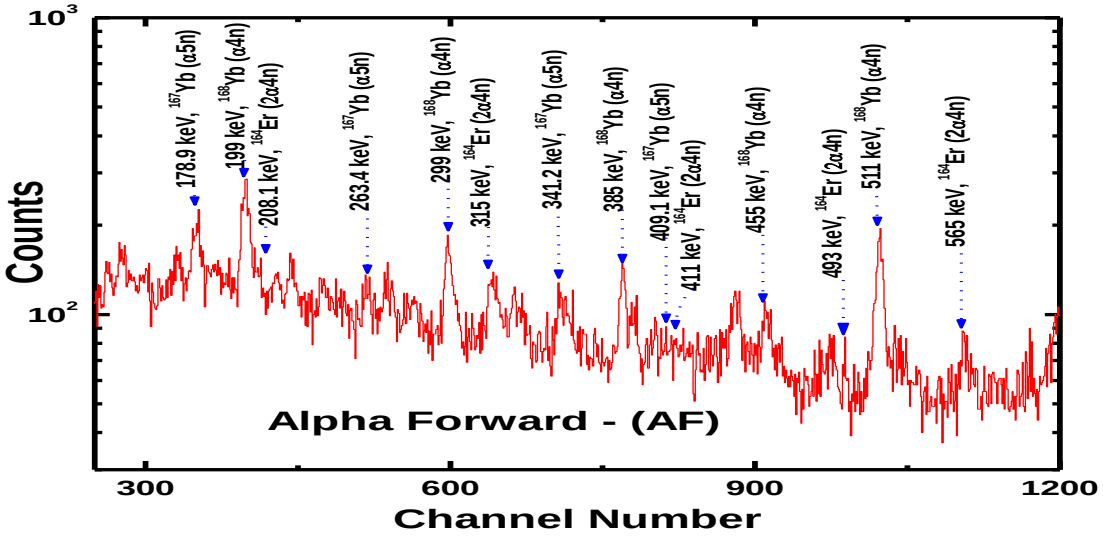

Fig. 4.7: A typical γ-ray spectrum in coincidence with fast α-particle in forward direction (10^0-60^0). The peaks have been assigned for the identification of fast α-emitting channels, which populated via ICF reaction dynamics.

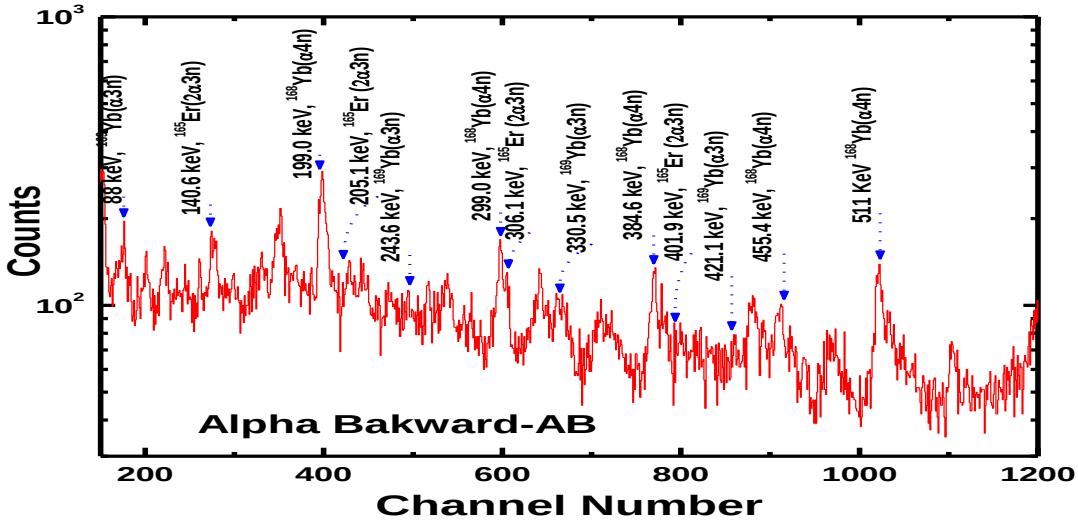

Fig. 4.8: A typical γ-ray spectrum in coincidence with evaporation α-particle in backward direction (120^0-170^0). The peaks have been assigned for the identification of evaporation (slow) α-emitting channels, which populated via CF reaction dynamics.

forward α-gated spectra. Moreover, ICF reaction products populated via αpxn/2αpxn channels have been identified from forward P-gated spectra. The intensity and area under the prompt gamma rays peak were used to calculate the production yield of the various residues populated through CF and/or ICF. In the present work, the γ-ray energy and their intensities have been taken from NNDC and RADWARE [3] level scheme directory and were used to determine the relative production yield for the observed spin. A typical γ-ray spectrum for ^{16}O + ^{160}Gd system recorded in singles mode is shown in Fig. 4.6, while the γ-ray spectrum in coincidence with α-particles gated in Forward angles (10^0-60^0) and Backward angles (120^0-170^0) are shown in Fig. 4.7 and 4.8 respectively.

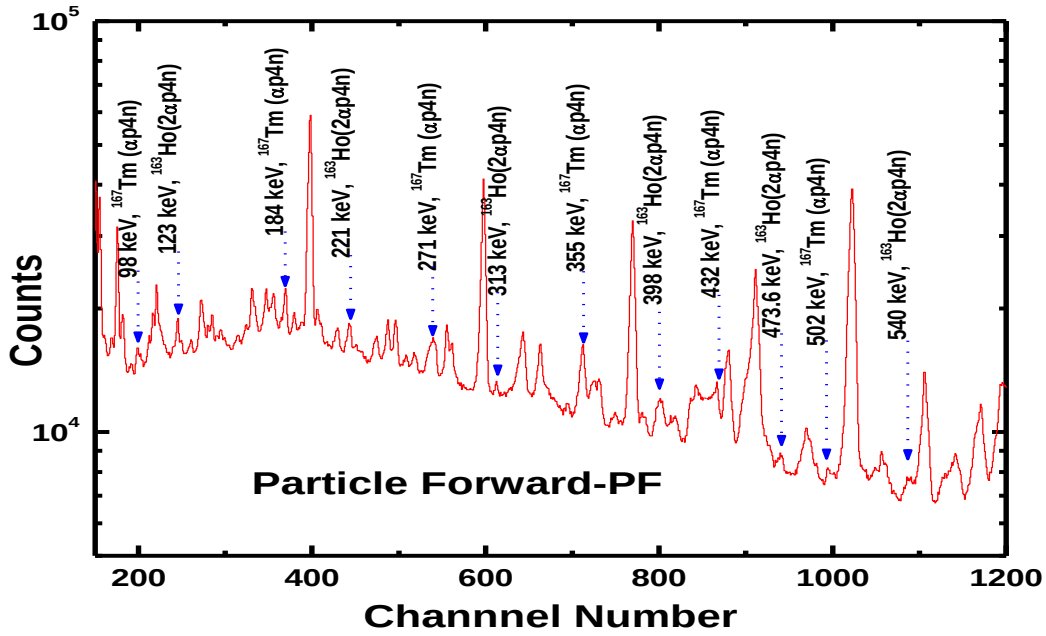

Fig. 4.9: A typical γ-ray spectrum in coincidence with particle in forward direction (10^0-60^0). The peaks have been assigned for the identification of αpxn channels, which populated via ICF reaction dynamics.

Spin distributions of different reaction products have been measured by studying the relative populations yields of different cascading levels in the rotational bands, based on the methodology adopted by Inamura *et al.*, [4] and Singh *et al.*, [5, 6]. The spin distributions of "direct" α-emitting channels (ICF) in the forward direction has been found to be distinctly different from those observed in CF channel. Identification of specific CF and ICF reaction channels in forward and backward angles were done by plotting the spin distributions or population yields of cascade gamma transitions of gated spectra of the rotational bands of different evaporation residues.

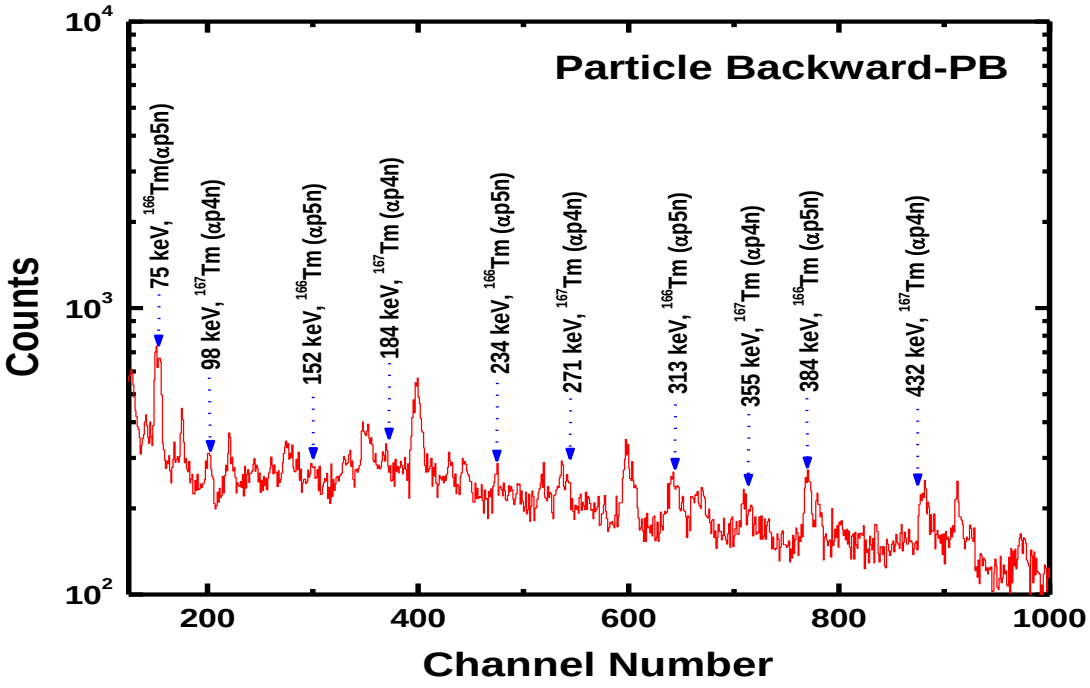

Fig. 4.10: A typical γ-ray spectrum in coincidence with particle in backward direction (120^0-170^0). The peaks have been assigned for the identification of αpxn channels, which populated via CF reaction dynamics.

4.2.1 Measurement of relative population yields and its interpretation

The reaction products populated via CF and ICF have been observed in the interaction of ^{16}O with ^{160}Gd at 5.6 MeV/ nucleon have been identified on the basis of entry state population in a residual nucleus prior to its de-excitation, which is expected to be entirely different in CF and ICF. In order to investigate, if the spin distributions for the evaporation residues produced via complete fusion (CF) and incomplete fusion (ICF) are same or different, feeding patterns of the rotational energy levels of the residual nuclei populated via CF and ICF of ^{16}O with ^{160}Gd have been studied by measuring the relative yields of the rotational levels from the intensities of gamma transitions for the evaporation residues using the particles and alphas-gated spectra imposing two gating conditions in 'forward' and 'backward' detectors. Eleven reaction residues ^{172}Hf (4n), ^{171}Hf (5n) and ^{170}Hf (6n), ^{169}Yb (α3n), ^{168}Yb (α4n), ^{167}Yb (α5n), ^{167}Tm (αp4n), ^{166}Tm (αp5n), ^{165}Er (2α3n), ^{164}Er (2α4n) and ^{163}Ho (2αp4n) have identified. The relative production yields for various CF and ICF reaction products have been plotted as a function of experimentally observed spin (J) corresponding to prompt γ-rays. As described earlier, the ICF reaction channels identified by the γ-transitions in coincidence with 'fast' α-particle(s) detected in 'forward cone' are: ^{168}Yb (α4n), ^{167}Yb (α5n), ^{164}Er (2α4n), ^{167}Tm (αp4n) and ^{163}Ho (2αp4n). Measured relative production yields as a function of observed spins (J), called 'spin distributions', have been displayed in Figs. 4.11(a)-(b). The spin distribution of the reaction products observed in ICF channels have been fitted by an analytical function of the following type, given by Barker *et al.*,[7]

$$Y = Y_0 /[1 + \exp(J - J_0)/\Delta] \qquad \ldots\ldots\ldots\ldots (4.1)$$

where; Δ is related to the width of mean input angular momentum J_0 and Y_0 is the normalization constant. J_0 is a sensitive parameter, which provides the qualitative information about the mean value of driving input angular momentum associated with various reaction products.

The relative production yields for evaporation residues ^{168}Yb (α4n), ^{167}Yb (α5n), (produced in 'forward' 1α-emission channels), as shown in Fig 4.11(a), have been found to be constant up to $J_0 \approx 9\hbar$ and then successively decreases exponentially with higher spin of the states, indicating hereby the absence of side-feeding to the lower members of yrast line transitions and the populations of low states are strongly hindered. Similarly, spin distributions of the residue ^{167}Tm (αp4n), as shown in Fig. 4.11(b), is observed in coincidence with 'fast' α-particle (P-gated) emitted in 'forward direction'. The intensity distribution of the cascade transitions of this evaporation residue is also found to be constant up to spin $J_0 \approx 9\hbar$, and then the yield successively decreases exponentially with high spin states. As such, the residues ^{164}Er (2α4n) and ^{163}Ho (2αp4n), (produced in 2α-emission channels) are also identified in 'fast' α–particles, ICF reaction channel gives $J_0 \approx 11\hbar$. The constancy of the relative yield for evaporation residue ^{164}Er (2α4n) and ^{163}Ho (2αp4n) (identified in forward cone 2α–emitting channel) has been observed to be extended up to about $J \approx 11\hbar$. It has been observed from the Figs. 4.11(a)-(b) that the spin at half-yield for 'fast' α– and 2α-emitting reaction channels (associated with ICF), observed in 'forward cone', comes out to be $J_0 \approx 9\hbar$ and $\approx 11\hbar$ respectively.

The neutrons channels ^{172}Hf (4n), ^{171}Hf (5n) and ^{170}Hf (6n) have been identified from "Singles spectra" and the spin distributions for neutron channels [associated with 'fusion-evaporation' (CF) channels] are displayed in Fig. 4.12. Their spin distributions show a sharp exponential fall in the intensities of cascade γ-transitions with higher spin of the states and give an indication of strong side-feeding to the lowest member of the yrast line transitions. Measured relative yields of each residue are fitted with least-square-fit straight lines. The spin at half-yield J_0 for these evaporation residues produced through CF reaction channels is found to be $J_0 \approx 7\hbar$. Moreover, reaction products identified in 'backward cone' gated spectra are ^{168}Yb (α4n), ^{165}Er (2α3n), ^{169}Yb (α3n), ^{166}Tm (αp5n) and ^{167}Tm (αp4n) and their spin distributions are displayed in Fig. 4.13(a)-(b). The lines through the experimental points are the results of the best fit to these data

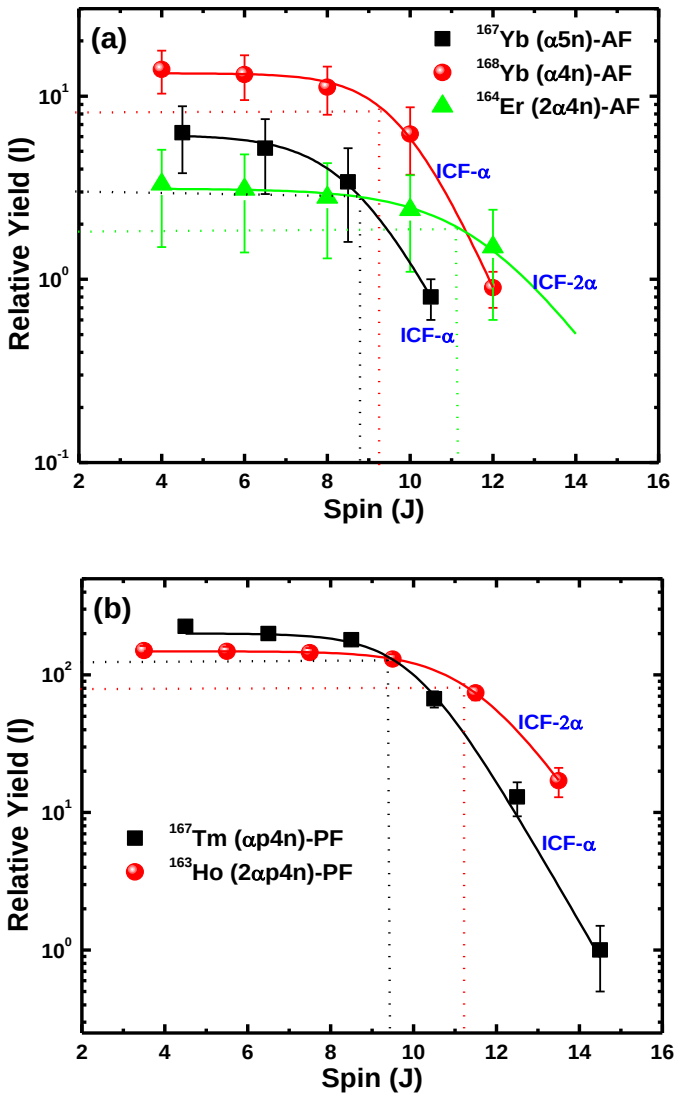

Fig. 4.11: The experimentally measured spin distributions of ERs ^{167}Yb, ^{168}Yb, ^{164}Er, (from α-gated spectra in forward direction), ^{167}Tm and ^{163}Ho (from P-gated spectra in forward direction) populated via ICF channels in ^{16}O + ^{160}Gd system at energy, E ~ 5.6 MeV/nucleon.

points. It is worth to mention that α–particles in 'backward direction' are 'evaporation' α–particlesi.e., CF α–particles). As can be seen clearly from the Figs.4.13(a)-(b), the spin distribution plots of the residues ^{169}Yb (α3n), ^{168}Yb (α4n), ^{167}Tm (αp4n), ^{166}Tm (αp5n) , ^{165}Er (2α3n), identified from 'backward α–gated' spectra, have been found to be distinctly different from those identified from 'forward α–gated' spectra, observed in ICF channels. The spin distributions of the above mentioned residues identified from 'backward α–gated' spectra follow the similar trend as has been observed in CF channels (i.e., in *xn* channels), displayed in Fig. 4.12.

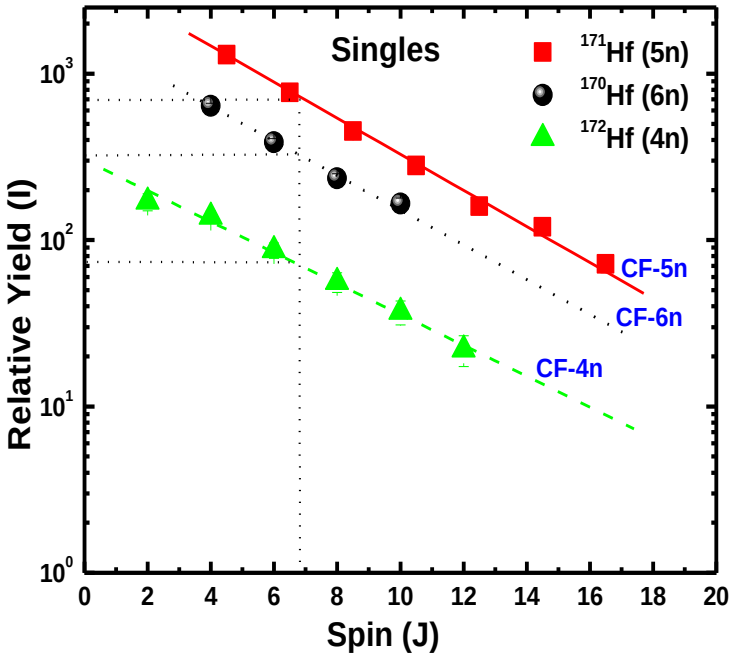

Fig. 4.12: The experimentally measured spin distribution of ERs ^{172}Hf, ^{171}Hf and ^{170}Hf (from Singles spectra) populated via (fusion evaporation) CF channels in ^{16}O + ^{160}Gd reactions at energy, E ~ 5.6 MeV / nucleon.

The spin at half-yield J_0 for these evaporation residues produced through CF reaction channels is found to be $J_0 \approx 7\hbar$ while the spin at half-yield J_0 for the residues produced through ICF reaction channels in 'fast' 1α and 2α– emission in 'forward cone', comes out to be $J_0 \approx 9\hbar$ and $\approx 11\hbar$ respectively. Present observations clearly show that the production of 'fast' α–particle(s) are at relatively higher input angular momentum and hence leads to peripheral interaction. It is also observed from the deduced value of J_0 that the multiplicity of 'fast' α-particles increases with the driving input angular momentum and shows the variation of ℓ-bins with different values of impact parameters at a given projectile energy. Moreover, it may also be inferred that lower ℓ values do not contribute to the ICF and small values of mean input angular momentum indicate the involvement of less input angular momentum in CF as compared to ICF reaction. It can be observed from Figs 4.11(a)-(b) that spin distribution of reaction products populated via 1α and 2α– emission channels, which have been identified from α-gated and Particle-gated spectra in forward direction are distinctly different from CF reaction products. It can also be observed from Figs 4.11-4.13 that there is remarkable difference in the measured spin distributions of different reaction products expected to be populated via CF and ICF reactions, which indicates that there is an involvement of entirely different reaction dynamics in the production of these reaction products. It can be observed from the neutron channels viz., ^{172}Hf (4n), ^{171}Hf (5n) and ^{170}Hf (6n), intensity of neutron channels falls off quickly with observed spin or intensity increasing steeply towards band head, which indicates a strong side-feeding during the de-excitation of compound nucleus. This may be because of the facts that CF process leads to the formation of compound nucleus in definite excitation energy (E^*) and a broad spin states population does exist. In the neutron channel products, yrast states are expected to be fed over broad spin range.

In order to have a better insight into the spin distributions of α-emitting channels, i.e. the residue ^{168}Yb (α4n) identified from forward α-gated spectrum (ICF

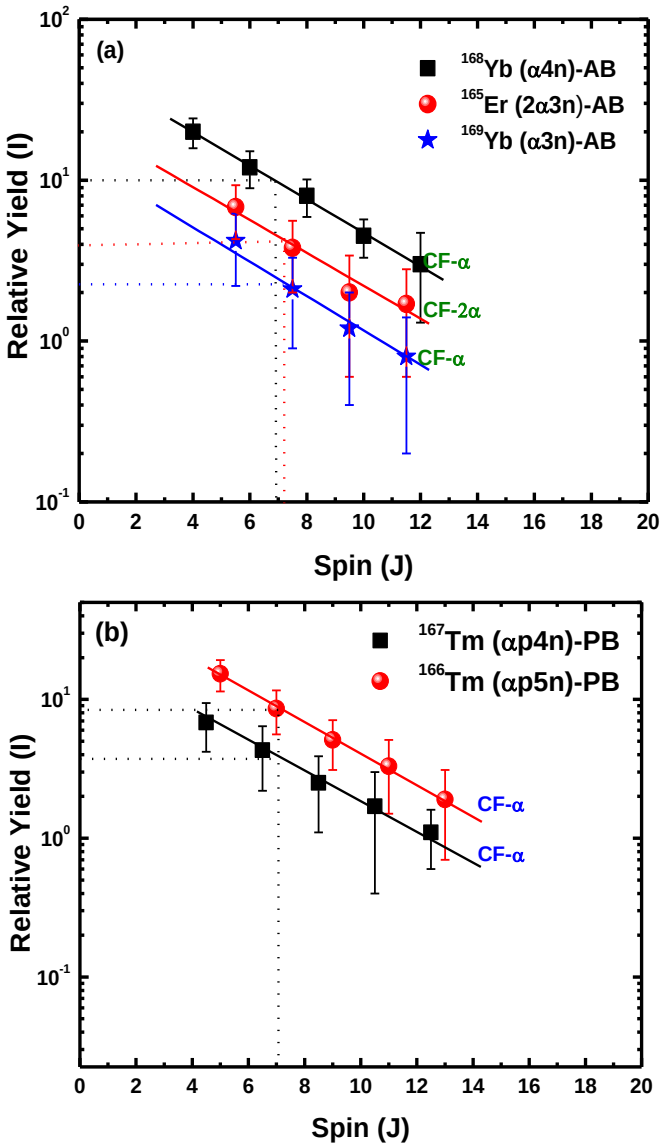

Fig. 4.13: The experimentally measured spin distributions of ERs populated via CF channels in ^{16}O + ^{160}Gd system at energy, E ~ 5.6 MeV/nucleon; (a) ^{168}Yb, ^{167}Yb and ^{165}Er (from α-gated spectra in backward direction); (b) ^{166}Tm and ^{167}Tm (from P-gated spectra in backward direction).

product) and backward α-gated spectrum (CF product), shown in Fig. 4.11(a) and Fig. 4.13(a) are compared. It can be observed from these figures, that spin distribution of ICF reaction product is found to be distinctly different than that of CF reaction product. It may be further pointed out that yield of the residue ^{168}Yb identified from forward-α-gated spectrum is found to increase towards the band head up to certain value of observed spin and then almost constant up to a lowest observed spin, while yield of the residue ^{168}Yb, identified from backward-α-gated (CF product) spectrum is found to fall steeply with the observed spin, which clearly indicates that strong side feeding to lower members of the yrast line transition as expected for CF reaction product. This clearly indicates that the given residue ^{168}Yb (α4n) is populated via two different routes like CF and ICF.

From the measured spin distribution profiles of the ERs populated in CF and ICF reactions as shown in Figs 4.11-4.13, it has been observed that the mean input angular momentum for ERs produced through CF reaction channels is found to be $\approx 7\hbar$ while the mean input angular momentum for ERs produced through ICF reaction channels in 'fast' α and 2α– emission in 'forward cone' of the CPDA, comes out to be $\approx 9\hbar$ and $\approx 12\hbar$ respectively. Present observations clearly show that the production of 'fast' α–particle(s) are at relatively higher input angular momentum and hence lead to peripheral interaction. An approximate relation has been obtained in terms of driving input angular momentum for CF and ICF reaction products with different α-multiplicity.

$$\ell_{ICF-2\alpha xn} \approx 1.22\,\ell_{ICF-\alpha xn} \approx 1.56\,\ell_{CF-xn/\alpha xn} \qquad \text{.....(4.2)}$$

The mean input angular momentum associated with xn, 1α and 2α-emission channels in forward direction have been plotted as a function of reaction mode and shown in Fig. 4.14. This figure shows that more and more angular momentum is involved with incompleteness of the system. It may also be pointed out from this figure that angular momentum associated with ICF reaction is larger than that of CF reaction.

Thus ICF reaction can be used to produce the nuclei in high spin states, which can not be achieved via CF process.

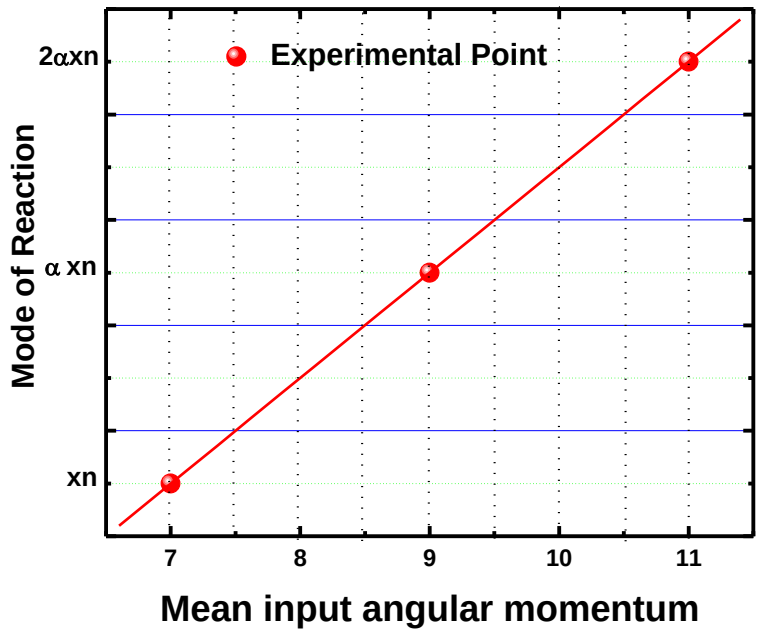

Fig. 4.14: The typical plot shows the dependence reaction mode on mean input angular momentum for ^{16}O + ^{160}Gd system at energy, E ~5.6 MeV/ nucleon.

4.2.2 Feeding intensity pattern in complete and incomplete fusion

As we have observed from spin distribution of the different reaction products populated via CF and /or ICF dynamics that intensity of yrast line transition decreases gradually with transition spin for CF process. This clearly indicates the broad side-feeding for yrast states in case of CF process While in ICF reaction products; intensity is almost constant up to certain transition spin and then decreases rapidly for the transition of high spin states. Hence, in ICF reactions, side-feeding distribution must have narrow window thereby indicates a well localized angular momentum region, where projectile

fragmentation takes place in the nuclear field of the target nucleus in contrast to large angular momentum window that involved in the CF reaction. To have a clear picture of strong feeding in CF and less feeding in ICF reactions, direct feeding intensity of γ–cascades of different ERs observed in CF and ICF reaction channels, estimated from experimentally measured spin distributions, have been plotted and displayed in Figs. 4.15 and 4.16(a)-(b). Fig. 4.15 shows direct feeding intensity plots of CF reaction channels, observed in neutron emission and backward-gated α– and 2α– emission channels. The figure shows that feeding intensity increases exponentially towards lower spin states, revealing strong feeding towards band head, as expected from CF dynamics, where band is fed over a broad spin range.

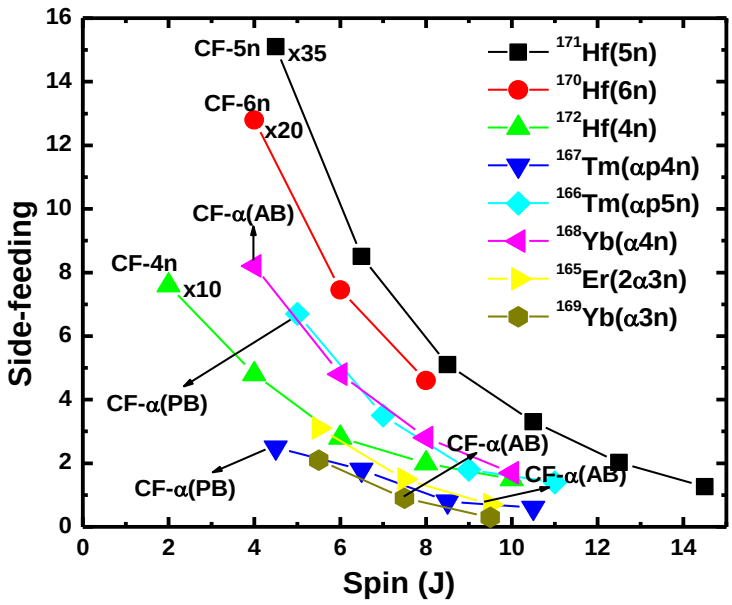

Fig. 4.15: Side-feeding intensities in the yrast band for all CF channels (identified from singles spectra, α and P-gated spectra in backward direction) populated via CF channels in $^{16}O + ^{160}Gd$ at energy, E ~5.6 MeV / nucleon.

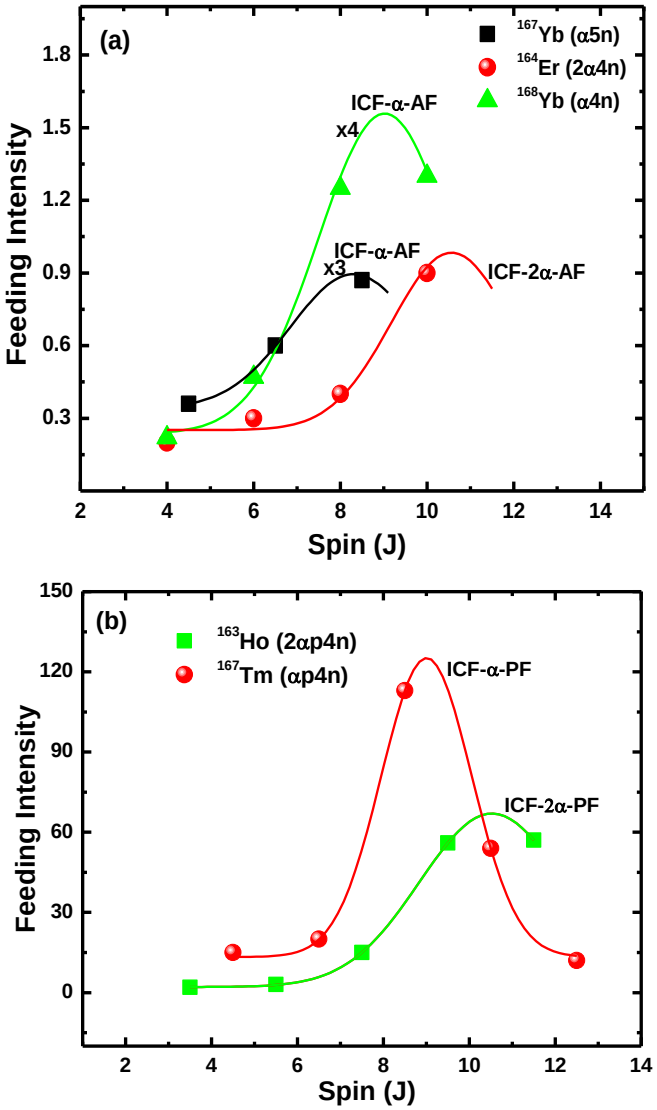

Fig. 4.16: Side-feeding intensities in the yrast band of ERs ^{167}Yb, ^{168}Yb, ^{164}Er, (deduced from spin distribution of α-gated spectra in forward direction) ^{167}Tm and ^{163}Ho (deduced from particle gated spectra in forward direction) populated via ICF channels in ^{16}O + ^{160}Gd system at energy, E ~5.6 MeV/nucleon.

On the other hand Fig. 4.16 (a)-(b) shows the direct feeding intensity of ICF reaction channels observed in forward gated α and 2α–emission channels (in alpha and particle spectra). The figure shows an exponential rise up to certain *J* values and then found to decrease towards higher spin states. This may be due to less feeding probability in ICF processes caused by de-excitation of the residual nucleus. The feeding intensity pattern in CF may be understood, as neutron emission carry negligible amount of angular momentum from compound nucleus, while emission of α-particle in forward cone takes significant amount of angular momentum and excitation energy, which hindered the population of low spin states. Finally, we conclude that in CF and ICF reaction products entirely different de-excitation patterns towards band head are involved with different input angular momentum. The present measurement may be used in developing a model for incomplete fusion dynamics, below 10 MeV/nucleon energy.

References:

[1] R. K. Bhowmik; IUAC, New Delhi, India (private communication).

[2] R. K. Bhowmik, *et al.*, Nucl. Phys. Symp. V **34B** (1991) 419; Nucl. Phys. Symp. V **44B** (2001) 422.

[3] RADWARE; the level scheme directory on http://radware.phy.ornl.gov/agsdir1/html, and National Nuclear Data Centre (NNDC).

[4] T. Inamura, M. Ishihara, T. Fukuda, T. Shimoda and H. Hiruta; Phys. Lett. **68B** (1977) 51.

[5] D. Singh, R. Ali, M.Afzal Ansari, K. Surendra Babu, P. P. Singh, M. K. Sharma, B. P. Singh, R. K. Sinha, Rakesh Kumar, S. Muralithar, R. P. Singh and R. K. Bhowmik; Phys. Rev. C **81** (2010) 027602.

[6] Pushpendra P. Singh, B. P. Singh, M. K. Sharma, Unnati Gupta, Rakesh Kumar, D. Singh, R. P. Singh, S. Murlithar, M. Afzal Ansari, R. Prasad and R. K. Bhowmik; Phys. Lett. B **671** (2009) 20.

[7] J. H. Barker, J. R. Beene, M. L. Harbert, D. C. Hansley, M. Jasskelainen, D. J. Sarantities, and R. Woodward; Phys. Rev. Lett. **45** (1980) 424.